

# An Evidence of Mass Dependent Differential Kinetic Freeze-out Scenario Observed in Pb-Pb Collisions at 2.76 TeV

Hai-Ling Lao<sup>a</sup>, Hua-Rong Wei<sup>a</sup>, Fu-Hu Liu<sup>a,1</sup>, and Roy A. Lacey<sup>b,2</sup>

<sup>a</sup>*Institute of Theoretical Physics, Shanxi University, Taiyuan, Shanxi 030006, China*

<sup>b</sup>*Departments of Chemistry & Physics, Stony Brook University, Stony Brook, NY 11794, USA*

**Abstract:** Transverse momentum spectra of different particles produced in mid-rapidity interval in lead-lead (Pb-Pb) collisions with different centrality intervals, measured by the ALICE Collaboration at center-of-mass energy per nucleon pair  $\sqrt{s_{NN}} = 2.76$  TeV, are conformably and approximately described by the Tsallis distribution. The dependences of parameters (effective temperature, entropy index, and normalization factor) on event centrality and particle rest mass are obtained. The source temperature at the kinetic freeze-out is obtained to be the intercept in the linear relation between effective temperature and particle rest mass, while the particle transverse flow velocity is approximately extracted to be the slope in the linear relation between mean transverse momentum and particle rest mass. It is shown that the source temperature increases with increase of particle rest mass, which exhibits an evidence of mass dependent differential kinetic freeze-out scenario or multiple kinetic freeze-out scenario.

**Keywords:** Source temperature, kinetic freeze-out scenario, mass dependent differential kinetic freeze-out scenario

**PACS:** 12.38.Mh, 25.75.Dw, 24.10.Pa

## 1 Introduction

High energy nucleus-nucleus (heavy ion) collisions at the large hadron collider (LHC) [1–5] have been providing another excellent environment and condition of high temperature and density, where the new state of matter, namely the quark-gluon plasma (QGP) [6, 7], is expected to form and to live for a longer lifetime than that at the relativistic heavy ion collider (RHIC) [8]. Although the RHIC is scheduled to run at lower energies (around the critical energy of phase transition from hadronic matter to QGP), the LHC is expected to run at higher energies. Presently, the LHC has provided three different types of collisions: proton-proton ( $pp$ ), proton-lead ( $p$ -Pb), and lead-lead (Pb-Pb) collisions at different collision energies. The former two are not expected to form the QGP due to small system, though the deconfinement of quarks and gluons may appear. The latter one is expected to form the QGP due to large system and high energy.

---

<sup>1</sup>E-mail: fuhuliu@163.com; fuhuliu@sxu.edu.cn

<sup>2</sup>E-mail: Roy.Lacey@Stonybrook.edu

It is believed that the QGP is formed in Pb-Pb collisions at the LHC and in nucleus-nucleus collisions at lower energy till dozens of GeV at the RHIC [9, 10]. If mesons are produced in the participant region where violent collision had happened and the QGP is formed, nuclear fragments such as helium or heavier nuclei are expected to emit in spectator region where non-violent evaporation and fragmentation had happened [11–13]. The ALICE Collaboration [14, 15] measured together positive pions  $\pi^+$ , positive kaons  $K^+$ , protons  $p$ , deuterons  $d$ , and one of helium isotopes  $^3\text{He}$  in Pb-Pb collisions with different centrality intervals at the LHC. It gives us a chance to describe uniformly different particles. In particular, we are interested in the uniform description of transverse momentum spectra of  $\pi^+$ ,  $K^+$ ,  $p$ ,  $d$ , and  $^3\text{He}$ , so that we can extract the kinetic freeze-out (KFO) temperature of interacting system (i.e. source temperature at KFO).

From source temperature at KFO, we can draw a KFO scenario. There are three different KFO scenarios discussed in literature [3, 16–19]. The single KFO scenario [16] uses one set of parameters for both the spectra of strange and non-strange particles. The double KFO scenario [3, 17] uses a set of parameters for the spectra of strange particles, and another set of parameters for the spectra of non-strange particles. The multi-KFO scenario [18, 19] uses different sets of parameters for different particles with different masses. Naturally, the mass dependent differential KFO scenario [19] belongs to the multi-KFO scenario. It is an open question which KFO scenario describes correctly. We are interested in the study of KFO scenario in the present work. As can be seen from the following sections, our analysis provides an evidence of mass dependent differential KFO scenario.

To extract source temperature at the KFO, we have to describe transverse momentum spectra. More than ten functions are used in the descriptions of transverse momentum spectra. In the present work, we select the Tsallis distribution [20–22] that covers the sum of two or three standard distributions [23, 24] and describes temperature fluctuations among different local equilibrium states. Based on the descriptions of the experimental data of the ALICE Collaboration [14, 15] on Pb-Pb collisions at center-of-mass energy per nucleon pair  $\sqrt{s_{NN}} = 2.76$  TeV, the source temperature at the KFO is obtained to be the intercept in the linear relation between effective temperature and particle rest mass, while the particle transverse flow velocity is approximately extracted to be the slope in the linear relation between mean transverse momentum and particle rest mass. If we use other functions, the method is in fact the same. Because of no difference between positive and negative spectra being reported [15], we are just fitting the available positive data in the analysis.

The structure of the present work is as followings. The model and method are shortly described in section 2. Results and discussion are given in section 3. In section 4, we summarize our main observations and conclusions.

## 2 The model and method

We discuss the collision process in the framework of the multisource thermal model [25–27]. According to the model, many emission sources are formed in high energy nucleus-nucleus collisions. We can choose different distributions to describe the emission sources

and particle spectra. These distributions include, but are not limited to, the Tsallis distribution [20–22], the standard (Boltzmann, Fermi-Dirac, and Bose-Einstein) distributions [23], the Tsallis + standard distributions [28–33], the Erlang distribution [25], and so forth.

The Tsallis distribution covers two or three standard distributions. The Tsallis + standard distributions cover two or three Tsallis distributions [24]. It is needless to choose the standard distributions due to multiple sources (temperatures). It is also needless to choose the Tsallis + standard distributions due to not too many sources (temperatures). A middle way is to choose the Tsallis distribution which describes the temperature fluctuation in a few sources to give an average value. These sources with different excitation degrees can be naturally described by the standard distributions with different effective temperatures, which result in the multisource thermal model [25–27].

The Tsallis distribution has more than one function forms [20–22, 28–33]. We consider a simplified form of the joint unit-density function of transverse momentum ( $p_T$ ) and rapidity ( $y$ ),

$$\frac{d^2 N}{dy dp_T} = \frac{gV}{(2\pi)^2} p_T \sqrt{p_T^2 + m_0^2} \cosh y \left[ 1 + \frac{q-1}{T} \left( \sqrt{p_T^2 + m_0^2} \cosh y - \mu \right) \right]^{-q/(q-1)}, \quad (1)$$

where  $N$  is the particle number,  $g$  is the degeneracy factor,  $V$  is the volume of emission sources,  $T$  is the temperature which describes averagely a few sources (local equilibrium states),  $q$  is the entropy index which describes the degree of non-equilibrium among different states,  $\mu$  is the chemical potential which is related to  $\sqrt{s_{NN}}$  [34] and can be regarded as 0 at the LHC,  $m_0$  is the rest mass of the considered particle. Generally,  $gV/(2\pi)^2$  can be regarded as the normalization factor which is related to other parameters.

Eq. (1) results in the transverse momentum distribution as follows

$$f(p_T) = \frac{1}{N} \frac{dN}{dp_T} \propto p_T \sqrt{p_T^2 + m_0^2} \int_{y_{\min}}^{y_{\max}} \cosh y \left[ 1 + \frac{q-1}{T} \left( \sqrt{p_T^2 + m_0^2} \cosh y - \mu \right) \right]^{-q/(q-1)} dy, \quad (2)$$

where  $y_{\max}$  and  $y_{\min}$  denote the maximum and minimum rapidities, respectively. Similarly, Eq. (1) results in the rapidity distribution as follows

$$f(y) = \frac{1}{N} \frac{dN}{dy} \propto \cosh y \int_0^{p_{T \max}} p_T \sqrt{p_T^2 + m_0^2} \left[ 1 + \frac{q-1}{T} \left( \sqrt{p_T^2 + m_0^2} \cosh y - \mu \right) \right]^{-q/(q-1)} dp_T, \quad (3)$$

where  $p_{T \max}$  denotes the maximum transverse momentum. The validity of Eqs. (2) and (3) is obvious due to Eq. (1).

Further, the momentum ( $p$ ), energy ( $E$ ), and kinetic energy ( $E_{kin}$ ) distributions are

$$f(p) = \frac{1}{N} \frac{dN}{dp} \propto p^2 \left[ 1 + \frac{q-1}{T} \left( \sqrt{p^2 + m_0^2} - \mu \right) \right]^{-q/(q-1)}, \quad (4)$$

$$f(E) = \frac{1}{N} \frac{dN}{dE} \propto E \sqrt{E^2 - m_0^2} \left[ 1 + \frac{q-1}{T} (E - \mu) \right]^{-q/(q-1)}, \quad (5)$$

and

$$f(E_{kin}) = \frac{1}{N} \frac{dN}{dE_{kin}} \propto (E_{kin} + m_0) \sqrt{E_{kin}^2 + 2m_0 E_{kin}} \left[ 1 + \frac{q-1}{T} (E_{kin} + m_0 - \mu) \right]^{-q/(q-1)}, \quad (6)$$

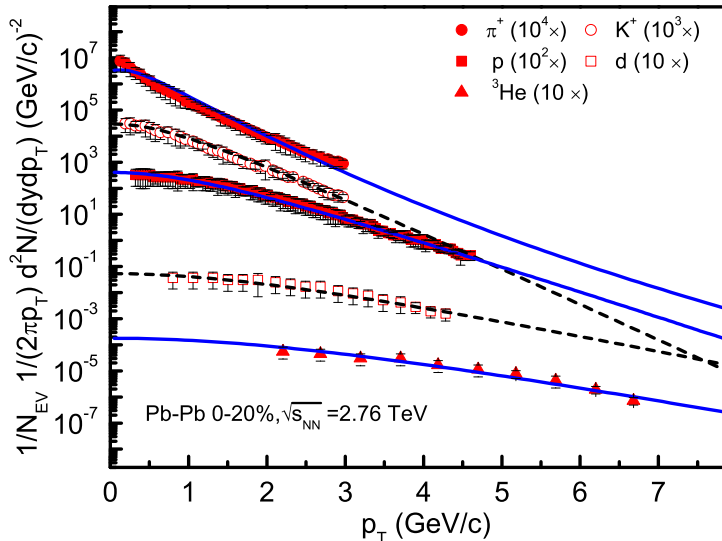


Figure 1. Transverse momentum spectra of  $\pi^+$ ,  $K^+$ ,  $p$ ,  $d$ , and  ${}^3\text{He}$  produced in mid-rapidity interval ( $|y| < 0.5$ ) in Pb-Pb collisions at  $\sqrt{s_{NN}} = 2.76$  TeV. The symbols represent the experimental data of the ALICE Collaboration [15] in centrality interval 0–20%, which are scaled by different amounts marked in the panel. The curves are our results fitted by using the Tsallis distribution and the method of least squares.

respectively. Based on Eq. (2) and a Monte Carlo calculation, the validity of Eq. (4) can be checked by the relation  $p = p_T / \sin \theta$  and the isotropic assumption for an emission source, where  $\theta$  denotes the emission angle of the considered particle. The validity of Eq. (5) can be checked by the relations  $E^2 = p^2 + m_0^2$  and  $|f(p)dp| = |f(E)dE|$  based on Eq. (4), where the latter one is used due to the probability conversation. And the validity of Eq. (6) can be checked by the relations  $E = E_{kin} + m_0$  and  $|f(E)dE| = |f(E_{kin})dE_{kin}|$  based on Eq. (5), where the latter one is used due to the same reason. Although Eqs. (3)–(6) are not used in the analysis, they are presented for complete representation and future application.

### 3 Results and discussion

Figure 1 presents the transverse momentum spectra,  $(1/N_{EV})d^2N/(2\pi p_T dy dp_T)$ , of  $\pi^+$ ,  $K^+$ ,  $p$ ,  $d$ , and  ${}^3\text{He}$  produced in mid-rapidity interval ( $|y| < 0.5$ ) in Pb-Pb collisions at  $\sqrt{s_{NN}} = 2.76$  TeV, where  $N_{EV}$  denotes the number of events. The symbols represent the experimental data of the ALICE Collaboration [15] in centrality interval 0–20%, which are scaled by different amounts marked in the panel. The curves are our results fitted by using the Tsallis distribution and the method of least squares. The values of related parameters,  $T$ ,  $q$ , and  $N_0$  (the normalization factor which is used to compare the normalized curve with experimental data), are listed in Table 1 with values of  $\chi^2$  per degree of

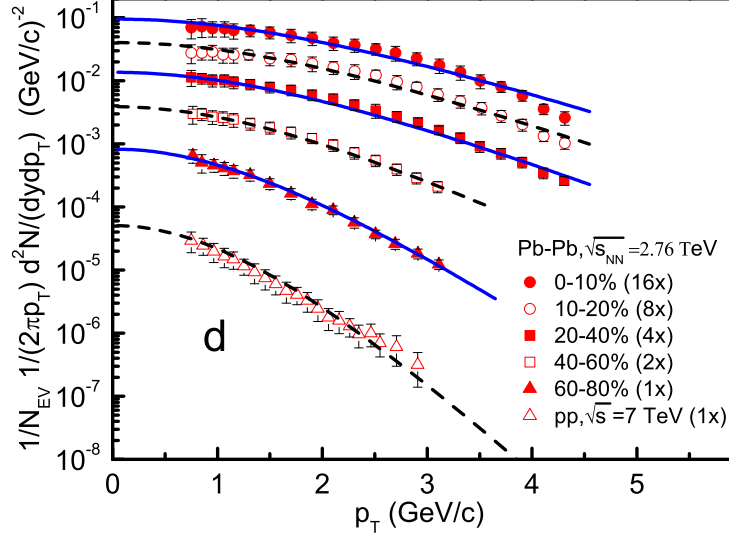


Figure 2. The same as for Figure 1, but showing the results of  $d$  in Pb-Pb collisions with different centrality intervals and in  $pp$  collisions.

freedom ( $\chi^2/\text{dof}$ ). One can see that the Tsallis distribution describes conformably and approximately  $\pi^+$ ,  $K^+$ ,  $p$ ,  $d$ , and  ${}^3\text{He}$  spectra. The effective temperature increases with increase of particle rest mass.

Table 1. Values of  $T$ ,  $q$ ,  $N_0$ , and  $\chi^2/\text{dof}$  corresponding to the curves in Figures 1–3, where the data set for  ${}^3\text{He}$  in Figure 1 is different from that for centrality interval 0–20% in Figure 3 [15], which renders different values of parameters.

Figure	Type	$T$ (GeV)	$q$	$N_0$	$\chi^2/\text{dof}$
Figure 1	$\pi^+$	$0.190 \pm 0.013$	$1.0380 \pm 0.0208$	$200.000 \pm 20.000$	3.689
	$K^+$	$0.297 \pm 0.027$	$1.0010 \pm 0.0200$	$23.400 \pm 3.510$	1.695
	$p$	$0.410 \pm 0.037$	$1.0010 \pm 0.0170$	$4.620 \pm 0.693$	0.191
	$d$	$0.650 \pm 0.072$	$1.0010 \pm 0.0200$	$0.010 \pm 0.003$	0.166
	${}^3\text{He}$	$0.720 \pm 0.058$	$1.0013 \pm 0.0160$	$(4.000 \pm 0.600) \times 10^{-5}$	2.723
Figure 2	0–10%	$0.700 \pm 0.050$	$1.0010 \pm 0.0070$	$(1.188 \pm 0.107) \times 10^{-2}$	1.425
	10–20%	$0.650 \pm 0.030$	$1.0010 \pm 0.0040$	$(9.500 \pm 0.950) \times 10^{-3}$	0.797
	20–40%	$0.600 \pm 0.030$	$1.0010 \pm 0.0190$	$(6.000 \pm 0.780) \times 10^{-3}$	0.604
	40–60%	$0.490 \pm 0.105$	$1.0010 \pm 0.0140$	$(2.950 \pm 0.220) \times 10^{-3}$	0.011
	60–80%	$0.355 \pm 0.079$	$1.0010 \pm 0.0100$	$(1.000 \pm 0.007) \times 10^{-3}$	1.731
	$pp$	$0.255 \pm 0.013$	$1.0010 \pm 0.0009$	$(5.000 \pm 0.650) \times 10^{-5}$	1.757
Figure 3	0–20%	$0.680 \pm 0.054$	$1.0040 \pm 0.0030$	$(6.100 \pm 0.793) \times 10^{-6}$	1.127
	20–80%	$0.750 \pm 0.016$	$1.0005 \pm 0.0004$	$(3.000 \pm 0.390) \times 10^{-5}$	0.929

Figure 2 is similar to Figure 1, but it shows the results for  $d$  in different centrality

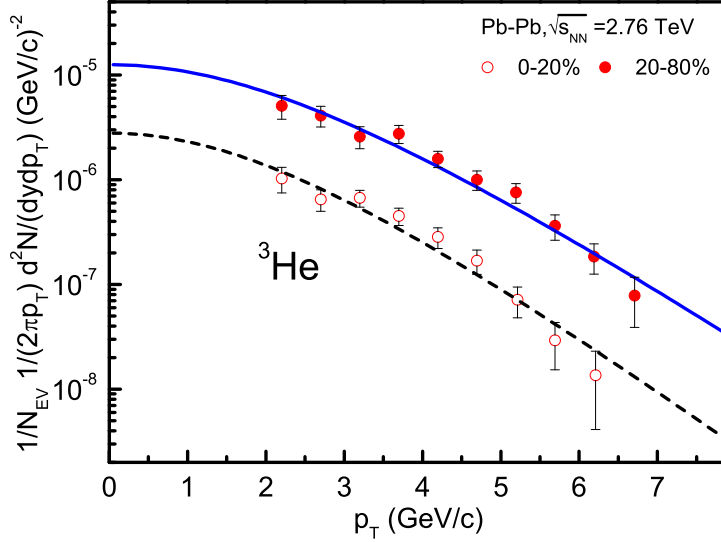


Figure 3. The same as for Figure 1, but showing the results of  ${}^3\text{He}$  in Pb-Pb collisions with two centrality intervals.

intervals, which are scaled by different amounts marked in the panels. At the same time, the result in  $pp$  collisions at  $\sqrt{s} = 7$  TeV is presented for comparison, where  $\sqrt{s}$  is a simplified form of  $\sqrt{s_{NN}}$  for  $pp$  collisions. Figure 3 is similar to Figure 1, but it shows the results for  ${}^3\text{He}$  in centrality intervals 0–20% and 20–80%, where the data set for 0–20% is different from that for  ${}^3\text{He}$  in Figure 1 [15]. The related parameter values are listed in Table 1 with values of  $\chi^2/\text{dof}$ . One can see that the Tsallis distribution describes approximately the experimental data of  $d$  produced in Pb-Pb collisions with different centrality intervals at the LHC. The effective temperature extracted from  $d$  spectra decreases with decrease of centrality (or increase of centrality percentage).

To study the change trends of parameters with centrality interval ( $C$ ) of event and rest mass of particle, Figure 4 gives the dependences of (a)  $T$  on  $C$  for  $d$  in events with different centrality intervals and (b)  $T$  on  $m_0$  for particles in events with centrality interval 0–20%, where only the result for  $d$  in Figure 4(a) is available due to the experimental result [15]. The symbols represent the parameter values listed in Table 1 and the curves are our results fitted by the method of least squares. The curve in Figure 4(a) is described by

$$T = -(0.000050 \pm 0.000002)C^2 - (0.0015 \pm 0.0001)C + (0.692 \pm 0.001) \quad (7)$$

with  $\chi^2/\text{dof}=0.109$ , where  $T$  is in the units of GeV. The solid, dotted, and dashed curves in Figure 4(b) are linear fittings for i)  $\pi^+$ ,  $K^+$ , and  $p$ ; ii)  $\pi^+$ ,  $K^+$ ,  $p$ , and  $d$ ; and iii)  $\pi^+$ ,  $K^+$ ,  $p$ ,  $d$ , and  ${}^3\text{He}$ , which are described by

$$T = (0.155 \pm 0.006) + (0.275 \pm 0.010)m_0, \quad (8)$$

$$T = (0.160 \pm 0.005) + (0.264 \pm 0.005)m_0, \quad (9)$$

and

$$T = (0.199 \pm 0.036) + (0.204 \pm 0.022)m_0, \quad (10)$$

with  $\chi^2/\text{dof}=0.130, 0.160,$  and  $3.294,$  respectively, where  $m_0$  is in the units of  $\text{GeV}/c^2$ .

The intercept in Eq. (8) is regarded as the KFO temperatures [35–38] of emission source, which is  $0.155 \text{ GeV}$  corresponding to massless particles, when the source produces  $\pi^+, K^+, \text{ and } p$ . Including  $d$  causes a large intercept ( $0.160 \text{ GeV}$ ) in Eq. (9), while including  $d$  and  ${}^3\text{He}$  causes a larger intercept ( $0.199 \text{ GeV}$ ) in Eq. (10). Although the errors in intercepts are large, these results render that the KFO temperature increases with increase of particle rest mass. This is an evidence of mass dependent differential KFO scenario or multiple KFO scenario [18, 19].

The blast-wave model [39] gives the KFO temperature extracted from  $d$  spectra to be  $0.077\text{--}0.124 \text{ GeV}$  and from  ${}^3\text{He}$  spectra to be  $0.101 \text{ GeV}$  [15] which are less than the present work. In particular, the blast-wave model gives the KFO temperature in central collisions to be less than that in peripheral collisions [15], which is inconsistent with Figure 4(a) which shows an opposite result. Although the result of blast-wave model can be explained as that the interacting system in central collisions undergone a longer kinetic evolution which results in a lower KFO temperature comparing with peripheral collisions, the present result can be explained as that the interacting system in central collisions stayed in a higher excitation state comparing with peripheral collisions.

On the other hand, we have used an alternative method to extract indirectly the KFO temperature and flow velocity. The evidence coming from similar analyses in RHIC and LHC experiments [40, 41], where the fit parameters have been studied also against centrality, even down to data of  $d$ -nucleus or  $pp$  collisions, confirms that the KFO temperature in central collisions is less than that in peripheral collisions, which is inconsistent with the present work. For central and peripheral collisions, the relative size of KFO temperature obtained in the present work is similar to those of the chemical freeze-out temperature and effective temperature. We would like to point out that the present work is qualitatively consistent with ref. [16], where the Tsallis + blast-wave model is used at RHIC energy.

Although the interpretation of the Tsallis distribution is still controversial, at least in the field of concern here, it could be interesting to learn the behavior of non-additive entropy. In Figure 5, the dependences of (a)  $q$  on  $C$  for  $d$  in events with different centrality intervals and (b)  $q$  on  $m_0$  for different particles in events with centrality interval 0–20% are given, where only the result for  $d$  in Figure 5(a) is available due to the experimental result [15]. The symbols represent the parameter values listed in Table 1. For  $d$  in events with different centrality intervals, the values of  $q$  are foregone to be consistent with one, which are also shown by the horizontal line in the panel [Figure 5(a)]. For the events with centrality interval 0–20%,  $\pi^+$  corresponds to a larger  $q$  than others. This renders that the production of pions is more polygenetic than others. Because of the most values of  $q$  being small, the interacting system stays approximately in an equilibrium state.

In fact, the ranges of most  $p_T$  spectra considered in Pb-Pb collisions in the present work are narrow, which result mainly from the soft process which is a single source and can be described by the standard distribution. If we study wide  $p_T$  spectra, both the soft and hard processes have to be considered. We need two or three standard distributions, the standard distribution + a power law, or the Tsallis distribution with large  $q$  to describe the wide spectra. The situation for  $pp$  collisions is similar to Pb-Pb collisions. The

advantage of Tsallis distribution will appear in description of the wide spectra. For the narrow spectra, both the standard distribution and the Tsallis distribution with small  $q$  are satisfied. However, we use the Tsallis distribution due to its potential application in wide  $p_T$  spectra. In addition, the STAR experiment already tried a Tsallis-like study, publishing also a Tsallis + blast-wave model-based interpretation of their data [8]. The ALICE data, on the other hand, have been compared to a blast-wave + thermal-based fit [15]. In both cases the agreement is very good. These facts render that the Tsallis distribution has a wide application in high energy physics.

In Figure 6, the dependences of (a)  $N_0$  on  $C$  for  $d$  in events with different centrality intervals and (b)  $N_0$  on  $m_0$  for different particles in events with centrality interval 0–20% are given, where only the result for  $d$  in Figure 6(a) is available due to the experimental result [15]. The symbols represent the parameter values listed in Table 1. The curves are our results fitted by the method of least squares, which are described by

$$N_0 = (0.016 \pm 0.001) \exp[-(0.030 \pm 0.002)C] - (0.0010 \pm 0.0001) \quad (11)$$

and

$$N_0 = (547.849 \pm 71.220) \exp[-(5.809 \pm 0.116)m_0] \quad (12)$$

with  $\chi^2/\text{dof}=1.677$  and  $7.017$  respectively. It is shown that  $N_0$  decreases with decrease of centrality. The larger the particle rest mass is, the lower the production probability is. The large  $\chi^2/\text{dof}$  for Eq. (12) is explained due to small errors in  $N_0$ . Although  $N_0$  is only a normalization factor and the data are not cross-section, they are related to the volumes of sources producing different particles. Therefore, studying  $N_0$  dependence is significant.

To extract the transverse flow velocity, we display the dependence of mean transverse momentum ( $\langle p_T \rangle$ ) on  $m_0$  in Figure 7. The symbols represent the values of  $\langle p_T \rangle$  for different particles calculated according to the Tsallis distribution. The solid, dotted, and dashed curves in Figure 7 are linear fittings for i)  $\pi^+$ ,  $K^+$ , and  $p$ ; ii)  $\pi^+$ ,  $K^+$ ,  $p$ , and  $d$ ; and iii)  $\pi^+$ ,  $K^+$ ,  $p$ ,  $d$ , and  ${}^3\text{He}$ , which are described by

$$\langle p_T \rangle = (0.305 \pm 0.007) + (0.491 \pm 0.011)m_0, \quad (13)$$

$$\langle p_T \rangle = (0.294 \pm 0.009) + (0.517 \pm 0.008)m_0, \quad (14)$$

and

$$\langle p_T \rangle = (0.347 \pm 0.049) + (0.435 \pm 0.031)m_0, \quad (15)$$

with  $\chi^2/\text{dof}=0.050$ ,  $0.124$ , and  $0.970$ , respectively, where  $\langle p_T \rangle$  is in the units of  $\text{GeV}/c$ . From the consideration of dimension, the slopes in Eqs. (13)–(15) are regarded as the (average) transverse flow velocity, which is close to  $0.5c$ . Including  $d$  or  $d$  and  ${}^3\text{He}$ , one can see a small effect. The blast-wave model [39] gives the transverse flow velocity for  $d$  is  $0.38$ – $0.63c$  and for  ${}^3\text{He}$  is  $0.56$ – $0.57c$  [15] which is comparable with the present work.

It seems that the results (Figures 1–3) obtained by us have a somewhat worse agreement with data with respect to the blast-wave based model [15, 39]. The reason is that crude model description and less parameters are used in the present work. In addition, KFO temperatures are difficult to interpret, they are not the straightforward KFO, and



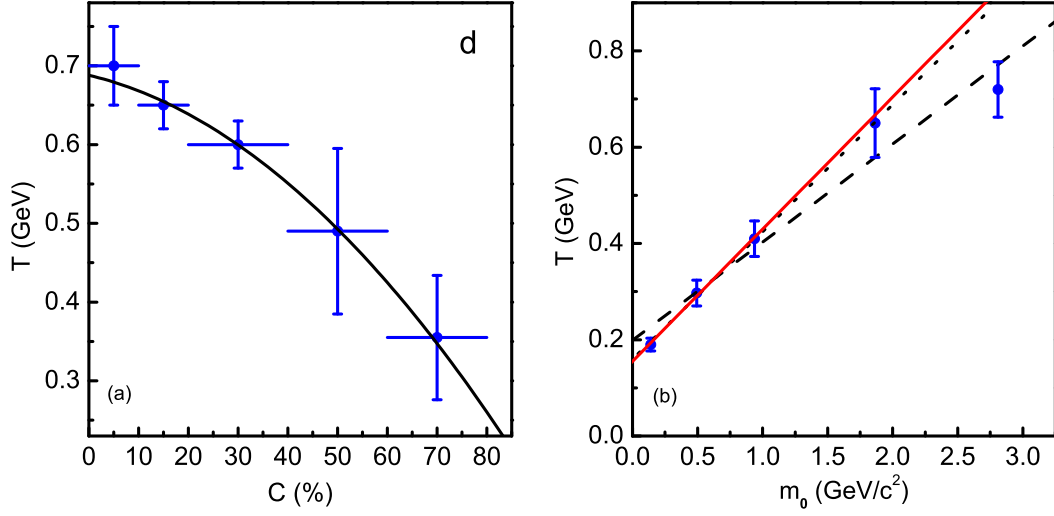


Figure 4. Dependence of (a)  $T$  on  $C$  for  $d$  in events with different centrality intervals and (b)  $T$  on  $m_0$  for particles in events with centrality interval 0–20%. The symbols represent the parameter values listed in Table 1 and the curves are our results fitted by the method of least squares.

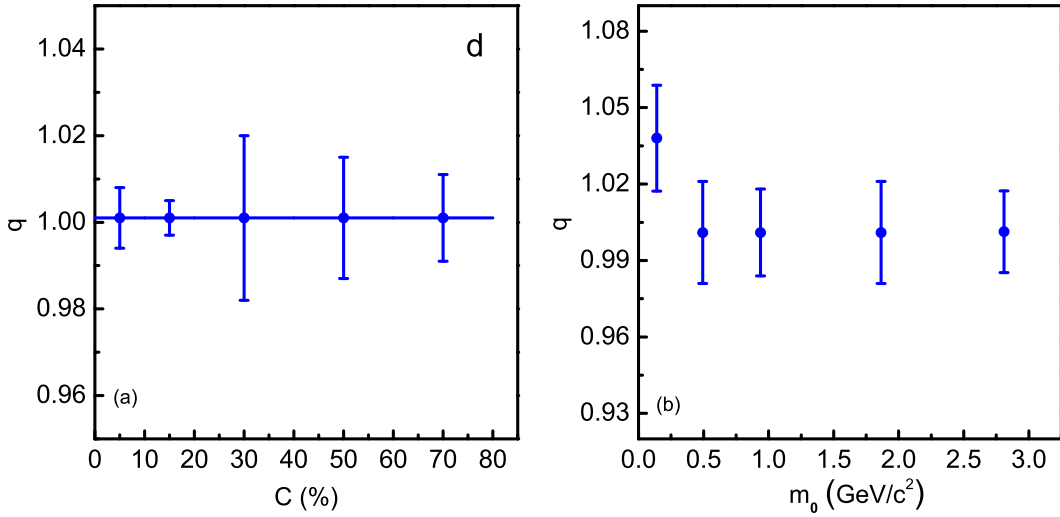


Figure 5. Dependence of (a)  $q$  on  $C$  for  $d$  in events with different centrality intervals and (b)  $q$  on  $m_0$  for particles in events with centrality interval 0–20%. The symbols represent the parameter values listed in Table 1. The horizontal line in Figure 5(a) indicates the same value of  $q$  with different uncertainties.

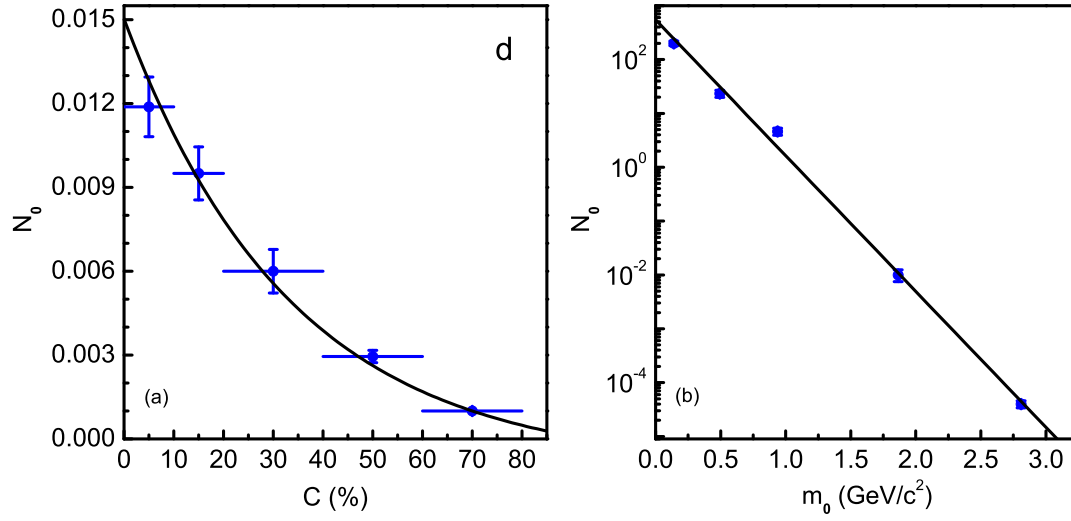


Figure 6. Dependence of (a)  $N_0$  on  $C$  for  $d$  in events with different centrality intervals and (b)  $N_0$  on  $m_0$  for particles in events with centrality interval 0–20%. The symbols represent the parameter values listed in Table 1. The curve and line are our results fitted by the method of least squares.

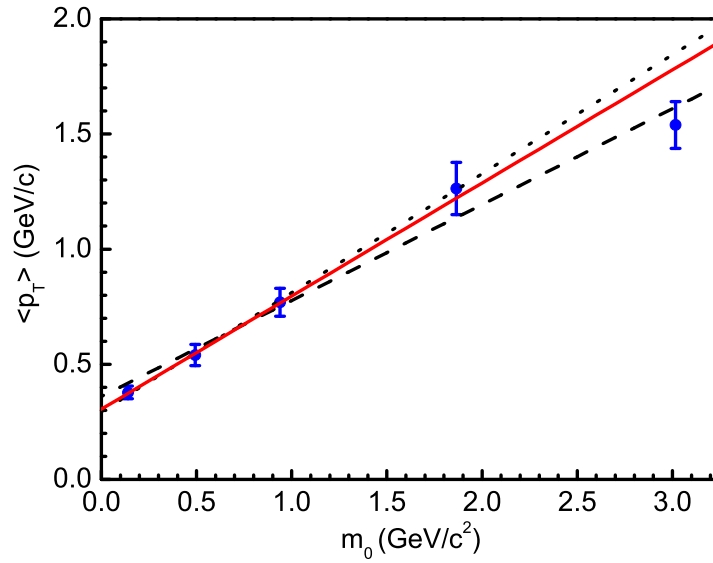


Figure 7. Dependence of  $\langle p_T \rangle$  on  $m_0$  for particles in events with centrality interval 0–20%. The symbols represent the values of  $\langle p_T \rangle$  calculated according to the Tsallis distribution. The curves are our results fitted by the method of least squares.

can be only extracted by indirect methods. Anyhow, the present work provides an alternative method to describe  $p_T$  spectra and to extract indirectly KFO temperature and flow velocity, though little inconsistency with other method [15] is existent. In fact, different functions result in different KFO temperatures. To extract the absolute temperature at KFO, the standard distribution is the best choice. However, we have to use a multi-component standard distribution.

In our very recent work [42], the linear relations between  $T$  and  $m_0$ ,  $T$  and mean moving mass  $\bar{m}$ ,  $\langle p_T \rangle$  and  $m_0$ ,  $\langle p_T \rangle$  and  $\bar{m}$ , mean momentum  $\langle p \rangle$  and  $m_0$ , as well as  $\langle p \rangle$  and  $\bar{m}$  are studied. It is shown that the intercept in the linear relation between  $T$  and  $m_0$  can be regarded as the KFO temperature, the slope in the linear relation  $\langle p_T \rangle$  and  $\bar{m}$  can be regarded as the transverse flow velocity, and the slope in the linear relation  $\langle p \rangle$  and  $\bar{m}$  can be regarded as the flow velocity. In the present work, we use an approximate treatment which regards the slope in the linear relation  $\langle p_T \rangle$  and  $m_0$  as the transverse flow velocity, which overestimates the value by a few percents.

## 4 Conclusions

We summarize here our main observations and conclusions.

The transverse momentum distributions of  $\pi^+$ ,  $K^+$ ,  $p$ ,  $d$ , and  ${}^3\text{He}$  produced in Pb-Pb collisions with different centrality intervals at the LHC are conformably analyzed by using the Tsallis distribution. The results calculated by us can fit approximately the experimental data of the ALICE Collaboration. The values of parameters such as the effective temperature, entropy index, and normalization factor are obtained.

The effective temperature extracted from transverse momentum spectra increases with increase of particle rest mass, and decreases with decrease of centrality. The kinetic freeze-out temperature of the interacting system in central collisions extracted from the intercept in the linear relation between effective temperature and particle rest mass for  $\pi^+$ ,  $K^+$ , and  $p$  is 0.155 GeV. The particle mass effects of kinetic freeze-out temperature for  $d$  and  ${}^3\text{He}$  are obvious. We have observed an evidence of mass dependent differential kinetic freeze-out scenario or multiple kinetic freeze-out scenario.

### Conflict of Interests

The authors declare that there is no conflict of interests regarding the publication of this paper.

### Acknowledgments

This work was supported by the National Natural Science Foundation of China under Grant No. 11575103 and the US DOE under contract DE-FG02-87ER40331.A008.

## References

- [1] J. Uphoff, O. Fochler, Z. Xu, and C. Greiner, “Open heavy flavor at RHIC and LHC in a partonic transport model,” *Acta Physica Polonica B Proceedings Supplement*, vol. 5, no. 2, pp. 555–560, 2012.
- [2] Y. Zhong, C.-B. Yang, X. Cai, and S.-Q. Feng, “A systematic study of magnetic field in relativistic heavy-ion collisions in the RHIC and LHC energy regions,” *Advances in High Energy Physics*, vol. 2015, Article ID 193039, 10 pages, 2015.
- [3] S. Chatterjee, S. Das, L. Kumar, D. Mishra, B. Mohanty, R. Sahoo, and N. Sharma, “Freeze-out parameters in heavy-ion collisions at AGS, SPS, RHIC, and LHC energies,” *Advances in High Energy Physics*, vol. 2015, Article ID 349013, 20 pages, 2015.
- [4] R. C. Hwa, “Recognizing critical behavior amidst minijets at the Large Hadron Collider,” *Advances in High Energy Physics*, vol. 2015, Article ID 526908, 10 pages, 2015.
- [5] G.-L. Ma and M.-W. Nie, “Properties of full jet in high-energy heavy-ion collisions from parton scatterings,” *Advances in High Energy Physics*, vol. 2015, Article ID 967474, 12 pages, 2015.
- [6] N. Itoh, “Hydrostatic equilibrium of hypothetical quark stars,” *Progress in Theoretical Physics*, vol. 44, no. 1, pp. 291–292, 1970.
- [7] T. D. Lee and G. C. Wick, “Vacuum stability and vacuum excitation in a spin-0 field theory,” *Physical Review D*, vol. 9, no. 8, pp. 2291–2316, 1974.
- [8] L. Adamczyk, J. K. Adkins, G. Agakishiev et al. (STAR Collaboration), “Measurements of dielectron production in Au+Au collisions at  $\sqrt{s_{NN}} = 200$  GeV from the STAR experiment,” *Physical Review C*, vol. 92, no. 2, Article ID 024912, 35 pages, 2015.
- [9] R. A. Lacey, “Indications for a critical end point in the phase diagram for hot and dense nuclear matter,” *Physical Review Letters*, vol. 114, no. 14, Article ID 142301, 5 pages, 2015.
- [10] M. Nasim, V. Bairathi, M. K. Sharma, B. Mohanty, and A. Bhasin, “A review on  $\phi$  meson production in heavy-ion collision,” *Advances in High Energy Physics*, vol. 2015, Article ID 197930, 16 pages, 2015.
- [11] R. J. Glauber, “High-energy collision theory,” in *Lectures of Theoretical Physics*, W. E. Brittin and L. G. Dunham, Eds., vol. 1, pp. 315–414, Interscience, New York, NY, USA, 1959.
- [12] M. I. Adamovich, M. M. Aggarwal, Y. A. Alexandrov et al. (EMU01 Collaboration), “Angular distributions of light projectile fragments in deep inelastic Pb+Em interactions at 160A GeV,” *The European Physical Journal A*, vol. 6, no. 4, pp. 421–425, 1999.

- [13] P. B. Price and Y. D. He, “Behavior of nuclear projectile fragments produced in collisions of 14.5A GeV  $^{28}\text{Si}$  with Pb and Cu targets,” *Physical Review C*, vol. 43, no. 2, pp. 835–848, 1991.
- [14] F. Barile (for the ALICE Collaboration), “Light (hyper-)nuclei production at the LHC measured with ALICE,” in *Proceedings of 3rd International Conference on New Frontiers in Physics*, Kolymbari, Crete, Greece, 28 July – 6 August, 2014.
- [15] J. Adam, D. Adamová, M. M. Aggarwal et al. (ALICE Collaboration), “Production of light nuclei and anti-nuclei in pp and Pb-Pb collisions at LHC energies,” Preprint CERN-PH-EP-2015-025, <http://arxiv.org/abs/1506.08951>, 2015.
- [16] Z. B. Tang, Y. C. Xu, L. J. Ruan, G. van Buren, F. Q. Wang, and Z. B. Xu, “Spectra and radial flow at RHIC with Tsallis statistics in a Blast-Wave description,” *Physical Review C*, vol. 79, no. 5, Article ID 051901(R), 5 pages, 2009.
- [17] S. Chatterjee, B. Mohanty, and R. Singh, “The freezeout hypersurface at LHC from particle spectra: Flavor and centrality dependence,” *Physical Review C*, vol. 92, no. 2, Article ID 024917, 10 pages, 2015.
- [18] S. Chatterjee and B. Mohanty, “Production of light nuclei in heavy ion collisions within multiple freezeout scenario,” *Physical Review C*, vol. 90, no. 3, Article ID 034908, 7 pages, 2014.
- [19] D. Thakur, S. Tripathy, P. Garg, R. Sahoo, and J. Cleymans, “Indication of a differential freeze-out in proton-proton and heavy-ion collisions at RHIC and LHC energies,” <http://arxiv.org/abs/1601.05223>, 2016.
- [20] C. Tsallis, “Possible generalization of Boltzmann-Gibbs statistics,” *Journal of Statistical Physics*, vol. 52, no. 1-2, pp. 479–487, 1988.
- [21] T. S. Biró, G. Purcsel, and K. Ürmösy, “Non-extensive approach to quark matter,” *The European Physical Journal A*, vol. 40, no. 3, pp. 325–340, 2009.
- [22] J. Cleymans and D. Worku, “Relativistic thermodynamics: transverse momentum distributions in high-energy physics,” *The European Physical Journal A*, vol. 48, Article ID 160, 8 pages, 2012.
- [23] P. Z. Ning, L. Li, and D. F. Min, *Foundation of Nuclear Physics: Nucleons and Nuclei*, Higher Education Press, Beijing, China, 2003.
- [24] F.-H. Liu, Y.-Q. Gao, and H.-R. Wei, “On descriptions of particle transverse momentum spectra in high energy collisions,” *Advances in High Energy Physics*, vol. 2014, Article ID 293387, 12 pages, 2014.
- [25] F.-H. Liu, Y.-Q. Gao, T. Tian, and B.-C. Li, “Unified description of transverse momentum spectrums contributed by soft and hard processes in high-energy nuclear collisions,” *The European Physical Journal A*, vol. 50, no. 6, Article ID 94, 9 pages, 2014.

- [26] F.-H. Liu and J.-S. Li, “Isotopic production cross section of fragments in  $^{56}\text{Fe}+p$  and  $^{136}\text{Xe}(^{124}\text{Xe})+\text{Pb}$  reactions over an energy range from  $300A$  to  $1500A$  MeV,” *Physical Review C*, vol. 78, no. 4, Article ID 044602, 13 pages, 2008.
- [27] F.-H. Liu, “Unified description of multiplicity distributions of final-state particles produced in collisions at high energies,” *Nuclear Physics A*, vol. 810, nos. 1–4, pp. 159–172, 2008.
- [28] F. Büyükkiliç and D. Demirhan, “A fractal approach to entropy and distribution functions,” *Physics Letters A*, vol. 181, no. 1, pp. 24–28, 1993.
- [29] J.-C. Chen, Z.-P. Zhang, G.-Z. Su, L.-X. Chen, and Y.-G. Shu, “q-generalized Bose-Einstein condensation based on Tsallis entropy,” *Physics Letters A*, vol. 300, no. 1, pp. 65–70, 2002.
- [30] J. M. Conroy and H. G. Miller, “Color superconductivity and Tsallis statistics,” *Physical Review D*, vol. 78, no. 5, Article ID 054010, 5 pages, 2008.
- [31] F. Pennini, A. Plastino, and A. R. Plastino, “Tsallis entropy and quantal distribution functions,” *Physics Letters. A*, vol. 208, nos. 4–6, pp. 309–314, 1995.
- [32] A. M. Teweldeberhan, A. R. Plastino, and H. G. Miller, “On the cut-off prescriptions associated with power-law generalized thermostatics,” *Physics Letters A*, vol. 343, nos. 1–3, pp. 71–78, 2005.
- [33] J. M. Conroy, H. G. Miller, and A. R. Plastino, “Thermodynamic consistency of the q-deformed Fermi-Dirac distribution in nonextensive thermostatics,” *Physics Letters A*, vol. 374, no. 45, pp. 4581–4584, 2010.
- [34] A. Andronic, P. Braun-Munzinger, and J. Stachel, “The horn, the hadron mass spectrum and the QCD phase diagram – the statistical model of hadron production in central nucleus-nucleus collisions,” *Nuclear Physics A*, vol. 834, nos. 1–4, pp. 237c–240c, 2010.
- [35] U. W. Heinz, “Concepts of heavy-ion physics,” *Lecture Notes for Lectures Presented at the 2nd CERN – Latin-American School of High-Energy Physics*, San Miguel Regla, Mexico, June 1-14, 2003, <http://arxiv.org/abs/hep-ph/0407360>, 2004.
- [36] S. S. Adler, S. Afanasiev, C. Aidala et al. (PHENIX Collaboration), “Identified charged particle spectra and yields in Au+Au collisions at  $\sqrt{s_{NN}} = 200$  GeV,” *Physical Review C*, vol. 69, no. 3, Article ID 034909, 32 pages, 2004.
- [37] S. Takeuchi, K. Murase, T. Hirano, P. Huovinen, and Y. Nara, “Effects of hadronic rescattering on multistrange hadrons in high-energy nuclear collisions,” *Physical Review C*, vol. 92, no. 4, Article ID 044907, 12 pages, 2015.
- [38] R. Russo, “Measurement of  $D^+$  meson production in p-Pb collisions with the ALICE detector,” Ph.D. thesis, Università degli Studi di Torino, Italy, 2015, <http://arxiv.org/abs/1511.04380>, 2015.

- [39] E. Schnedermann, J. Sollfrank, and U. W. Heinz, “Thermal phenomenology of hadrons from 200A GeV S+S collisions,” *Physical Review C*, vol. 48, no. 5, pp. 2462–2475, 1993.
- [40] J. Adams, M. M. Aggarwal, Z. Ahammed et al. (STAR Collaboration), “Experimental and theoretical challenges in the search for the quark-gluon plasma: The STAR Collaboration’s critical assessment of the evidence from RHIC collisions,” *Nuclear Physics A*, vol. 757, nos. 1–2, pp. 102–183, 2005.
- [41] B. Abelev, J. Adam, D. Adamová et al. (ALICE Collaboration), “Centrality dependence of  $\pi$ ,  $K$ , and  $p$  production in Pb-Pb collisions at  $\sqrt{s_{NN}} = 2.76$  TeV,” *Physical Review C*, vol. 88, no. 4, Article ID 044910, 23 pages, 2013.
- [42] H.-R. Wei, F.-H. Liu, R. A. Lacey, “Kinetic freeze-out temperature and flow velocity extracted from transverse momentum spectra of final-state light flavor particles produced in collisions at RHIC and LHC,” *The European Physical Journal A*, accepted, 2016.